ACS APPLIED MATERIALS & INTERFACES

Research Article

www.acsami.org

Surprisingly High Activity for Oxygen Reduction Reaction of Selected Oxides Lacking Long Oxygen-Ion Diffusion Paths at Intermediate Temperatures: A Case Study of Cobalt-Free $BaFeO_{3-\delta}$

Feifei Dong,[†,‡] Yubo Chen,[†,‡] Dengjie Chen,[†,‡] and Zongping Shao*[,†,§]

[†]State Key Laboratory of Materials-Oriented Chemical Engineering, Nanjing Tech University, Nanjing, Jiangsu 210009, P. R. China

[‡]College of Chemistry and Chemical Engineering, Nanjing Tech University, Nanjing, Jiangsu 210009, P. R. China

[§]College of Energy, Nanjing Tech University, Nanjing, Jiangsu 210009, P. R. China

Supporting Information

ABSTRACT: The widespread application of solid oxide fuel cell technology requires the development of innovative electrodes with high activity for oxygen reduction reaction (ORR) at intermediate temperatures. Here, we demonstrate that a cobalt-free parent oxide $BaFeO_{3-\delta}$ (BF), which lacks long-range oxygen-ion diffusion paths, has surprisingly high electrocatalytic activity for ORR. Both in situ high-temperature X-ray diffraction analysis on room-temperature powder and transmission electron microscopy on quenched powder are applied to investigate the crystal structure of BF. Despite the lack of long oxygen-ion diffusion paths, the easy redox of iron cations as demonstrated by thermal gravimetric analysis (TGA) and oxygen temperature-programmed desorption and the high oxygen vacancy concentration as supported by iodometric titration and TGA benefit the reduction of oxygen to oxygen ions. Moreover, the electrical conductivity relaxation technique in conjunction with a transient thermogravimetric study reveals very high surface exchange kinetics of BF oxide. At 700 °C, the area specific resistance of BF cathode, as expressed by a symmetrical cell configuration, is only ~0.021 Ω cm^2, and the derived single fuel cell achieves high power output with a peak power density of 870 mW cm^{-2}. It suggests that an undoped BF parent oxide can be used as a high-efficiency catalyst for ORR.

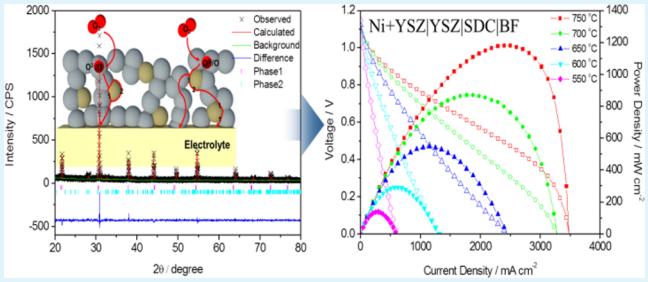

KEYWORDS: *solid oxide fuel cell, oxygen reduction reaction, $BaFeO_{3-\delta}$, oxygen vacancy, surface exchange kinetics*

1. INTRODUCTION

Electrochemical energy conversion has become one of the most efficient methods for energy utilization because it surpasses the efficiency limitation caused by the Carnot cycle in conventional thermal power processes. As a type of high-temperature electrochemical energy conversion devices, solid-oxide fuel cells (SOFCs) have the additional advantage of fuel flexibility.[1,2] A combination of SOFCs technology and renewable biofuels may provide an excellent choice for realizing sustainable energy systems in the future.[3]

A typical SOFC process involves the electrochemical reduction of molecular oxygen over the cathode (positive electrode) to oxygen ions, the incorporation of as-formed oxygen ions into the electrolyte bulk (assuming oxygen ions are the conducting species), the diffusion to the anode (negative electrode)-electrolyte interface, and the reaction of oxygen ions with fuel over the anode surface to generate electric power as well as heat in many cases. The power output of SOFCs is determined by the electrode polarization resistance and by the ohmic resistance of the electrolyte. Poor activity of the state-of-the-art cathode for the oxygen reduction reaction (ORR) has become the main obstacle to achieve high power density of SOFCs with practical importance at reduced temperatures.[4,5] The widespread application of SOFCs technology thus strongly relies on the development of highly efficient electrode materials for ORR.

During the past few decades, pure electron-conducting $La_{0.8}Sr_{0.2}MnO_{3-\delta}$ (LSM) perovskite oxide has been mainly applied as the cathode material of SOFCs,[6,7] and it has exhibited a negligible oxygen vacancy concentration and thus near-zero oxygen-ion conductivity under open circuit voltage (OCV) conditions. Under zero or small polarization conditions, the active sites for ORR of fuel cells with LSM electrode and $(ZrO_2)_{0.92}(Y_2O_3)_{0.08}$ (YSZ) electrolyte were mainly limited to the electrode (LSM)-electrolyte (YSZ)-gas (air) triple phase boundary (TPB) region. Under large polarization conditions, LSM may be partially reduced to introduce oxygen vacancies and thus oxygen-ion conductivity into the oxide bulk; the active reaction sites can then penetrate to a certain degree into the oxide bulk, thereby resulting in improved activity for ORR.[8] However, LSM still showed insufficient activity below 800 °C. It is generally believed that

Received: February 24, 2014
Accepted: June 30, 2014
Published: June 30, 2014

an increase in the oxygen-ion conductivity of electrode is beneficial for improving its ORR activity because the reaction sites can be extended into the bulk of electrode. Thus, introducing oxygen-ion conductivity into electrode material has become a general strategy for the development of new electrode materials with improved performance at reduced temperatures. One method involves the formation of a composite electrode consisting of LSM and an oxygen-ion conducting material such as YSZ in a mutually penetrative way.[9] Another method involves the development of a single phase oxide with mixed oxygen-ion and electronic conductivities, and a typical example is $Ba_{0.5}Sr_{0.5}Co_{0.8}Fe_{0.2}O_{3-\delta}$ (BSCF) oxide,[10,11] which exhibited superior activity for ORR at reduced temperatures (500−700 °C). Interestingly, the modification of $La_{0.6}Sr_{0.4}Co_{0.2}Fe_{0.8}O_{3-\delta}$ (LSCF) surface with less oxygen-ion conductive LSM oxide film resulted in a marked increase in activity for ORR at intermediate temperatures.[12] It implies that the surface activity sometimes also plays an important role in achieving high electrochemical activity of the electrode for ORR.

In this study, we reported that a surprisingly high activity for ORR can be achieved for some oxides with poor apparent oxygen-ion conductivity but a high concentration of oxygen vacancies in their lattice structures, which suggests that surface oxygen vacancies are sometimes more important than bulk oxygen-ion conductivity for ORR. Cobalt-free undoped $BaFeO_{3-\delta}$ (BF), a parent oxide for many composite oxides with diverse properties,[13−15] was specifically investigated. Under the operation conditions of SOFC cathode (550−750 °C and air atmosphere), BF exhibited oxygen nonstoichiometry δ as large as ∼0.55, but the oxygen ion was immobilized at temperatures up to 750 °C. However, an area specific resistance (ASR) of 0.011 Ω cm^2 and a peak power density (PPD) of 1180 mW cm^{-2} were reached at 750 °C when using BF as the oxygen reduction electrode. A detailed investigation was performed to demonstrate that the fast surface exchange kinetics, which was strongly related to the surface oxygen vacancy concentration, accounted for the superior performance. It thus provides a new strategy for the development of high performance oxygen reduction electrodes for SOFCs.

2. EXPERIMENTAL SECTION

2.1. Powder Preparation. All powders investigated were synthesized using a combined EDTA-citrate complexing sol−gel process. Analytic reagents of $Ba(NO_3)_2$, $Sr(NO_3)_2$, $La(NO_3)_3{\cdot}xH_2O$, $Fe(NO_3)_3{\cdot}xH_2O$, $Co(NO_3)_2{\cdot}xH_2O$, and $Mn(CH_3COO)_2{\cdot}4H_2O$ were used as the raw materials for metal sources. As such, $La(NO_3)_3{\cdot}xH_2O$, $Fe(NO_3)_3{\cdot}xH_2O$, and $Co(NO_3)_2{\cdot}xH_2O$ were first prepared in aqueous solution at concentrations of approximately 1 M, which were determined by the standard EDTA titration method, due to the uncertain amount of crystal water in their structures. Taking the preparation of BF as an example, stoichiometric amounts of the metal nitrates were mixed in deionized water and heated at 80 °C under stirring. The molar ratio of total metal nitrates, EDTA, and citric acid in the solution was 1:1:2. The pH of the solution was adjusted to ∼6 by adding $NH_3{\cdot}H_2O$ to ensure complete complexation. A transparent gel, which was attained after the evaporation of water, was pretreated at 250 °C in an oven to form a black solid precursor. The precursor was then calcined at 1000 °C for 5 h in air, resulting in the desired perovskite oxide.

2.2. Characterization. The crystal structures of the investigated powders were determined by X-ray diffraction (XRD), which was performed on a Rigaku Smartlab instrument using monochromator-filtered Cu Kα radiation. The data were collected in a step-scan mode within a range of 20−80° with intervals of 0.02°. A Philips X'Pert Pr X-ray apparatus with an in situ heating accessory (HT-XRD) was used to characterize the structural evolution of powders in an atmosphere of flowing air. The temperature was varied between room temperature and 1000 °C with a heating rate of 5 °C min^{-1}, and the sample was equilibrated for 15 min at the target temperature prior to each measurement. Rietveld refinements on the XRD patterns were carried out using General Structure Analysis System (GSAS) software. Transmission electron microscopy (TEM) was performed at 200 kV on a JEOL JEM-2100 field-emission instrument.

Oxygen permeation was measured in a high-temperature permeation device as detailed elsewhere.[16] Sintered disks, polished to 1 mm thickness, were sealed onto alumina tubes using silver paste (DAD-87, Shanghai, China). The feed side was fed with flow air, whereas helium served as the sweep gas at a flow rate of 100 mL min^{-1}. The flow rate was regularly calibrated using a bubble flow meter. The oxygen concentration of the outlet steam from the permeation side was analyzed by an online gas chromatograph (Varian, Walnut Creek, CA, CP 3800).

The oxygen nonstoichiometry (δ) and the average valence state of iron in BF at room temperature were measured by iodometric titration. Approximately 0.1 g of powdered sample was dissolved in an aqueous solution of KI with the help of added HCl. Reaction with iodide reduced iron ions, e.g., Fe^{4+} and/or Fe^{3+} to Fe^{3+} and/or Fe^{2+} with the simultaneous formation of I_2, the amount of which was quantified by titration with a standardized thiosulfate solution. The average iron cations valence and oxygen vacancy concentration were then calculated on the basis of the amount of I_2 formed.

The variations in the weight and oxygen nonstoichiometry of BF powder from room temperature to 1000 °C were measured by thermal gravimetric analysis (TGA) using an apparatus (Netzsch, STA 449 F3) with a ramping rate of 10 °C min^{-1} under air with a flow rate of 50 mL min^{-1}. For the transient TGA experiment, approximately 10 mg of the sample was heated from room temperature to 700 °C at a rate of 10 °C min^{-1} under pure nitrogen flow. When held at the desired temperature of 700 °C, the surrounding atmosphere swiftly changed to a nitrogen−oxygen mixture (∼0.21 atm) after the weight of the sample reached a stable state. Subsequently, a transient weight increase was recorded in the curve of the sample, which was subjected to a change of the surrounding gas (namely, oxygen absorption period).

The oxygen temperature-programmed desorption (O_2-TPD) test was performed on a homemade apparatus equipped with a mass spectrometer (MS, Hiden QIC-20). Pure argon was used as the carrier gas with a flow rate of 15 mL min^{-1}. A small granular 150 mg sample was pretreated under flowing argon at room temperature until the in situ monitored oxygen concentration reached a relatively steady state, and the temperature was then increased from room temperature to 930 °C at a rate of 10 °C min^{-1}.

The electrical conductivity relaxation (ECR) technique was performed to determine the oxygen bulk diffusion coefficient (D_{chem}) and the oxygen surface exchange coefficient (K_{chem}). After the sintered bar-shaped samples were stabilized for a certain period of time in a furnace at a certain temperature under a controlled atmosphere, a sudden change in the oxygen partial pressure, e.g., from 0.1 to 0.21 atm, was introduced by abruptly switching from the initial gas to another gas. The conductivity relaxation was measured as a function of time based on a four-probe DC configuration using a Keithley 2420 source meter. The test was conducted between 750 and 550 °C at an interval of 50 °C. After each change in temperature, the bar was stabilized for at least 1 h before the data were collected.

2.3. Fabrication of Symmetric Cells. Symmetrical cells with an electrode|$Sm_{0.2}Ce_{0.8}O_{1.9}$ (SDC)|electrode configuration were fabricated for electrochemical impedance studies. Dense SDC disks were prepared through dry pressing with subsequent calcination at 1400 °C for 5 h. Electrode slurries for spray deposition were prepared by dispersing the powder into a premixed solution of isopropyl alcohol, ethylene glycol, and glycerol, followed by milling (Fritsch, Pulverisette 6) at a rotating speed of 400 rpm for 0.5 h. The resulting slurries were sprayed onto both surfaces of the SDC disks in a symmetric configuration and subsequently fired at 1000−1100 °C for 2 h in air.

2.4. Fabrication of Anode-Supported SOFCs. Single cells with an anode-supported, thin-film dual-layer electrolyte configuration were prepared via a tape casting process, spray deposition, and subsequent high-temperature sintering. The details for preparing anode substrates NiO+ YSZ through the tape casting process are available in the literature.[17] The YSZ|SDC double electrolyte layers were prepared by wet powder spraying. The YSZ suspension was first sprayed onto the anode substrates followed by calcination at 1400 °C for 5 h, with the procedure subsequently repeated for the SDC suspension (buffering layer) deposited onto the dense YSZ surface and followed by calcination at 1350 °C for 5 h. The cathode slurries were then painted onto the central surface of the electrolytes and fired at 1000−1100 °C for 2 h in air.

2.5. Electrochemical Evaluation and Fuel Cell Testing. The electrochemical impedance spectra (EIS) of the symmetrical cells were acquired using Solartron 1287 and 1260A electrochemical workstations. The frequency range was 100 kHz to 0.01 Hz, and the signal amplitude was 10 mV under open cell voltage conditions. Fuel cells were constructed with a four-terminal configuration, and the $I-V$ polarization operated between 750 and 550 °C was measured using a Keithley 2420 source meter. Hydrogen fuel was fed into the anode chamber at a flow rate of 80 mL min^{-1}, and ambient air served as the oxidant gas in the cathode chamber.

3. RESULTS AND DISCUSSION

3.1. Basic Properties. $SrCoO_{3-\delta}$ (SC), $BaCoO_{3-\delta}$ (BC), $SrFeO_{3-\delta}$ (SF), and BF are the parent oxides for a wide range of perovskite oxides that possess several lattice structures, depending on the temperature, surrounding atmosphere, and thermal history. Shown in Figure 1 are the room-temperature

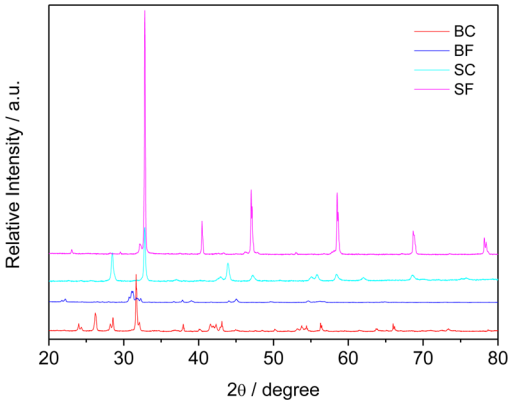

Figure 1. Room-temperature XRD patterns of BC, BF, SC, and SF powders from the sol−gel precursor calcined at 1000 °C for 5 h in air.

XRD patterns of four oxides synthesized from a sol−gel process after calcination at 1000 °C in air followed by cooling down naturally under the same atmosphere. All four samples exhibited diffraction peaks that were very different from those from a standard oxygen vacancy-disordered cubic perovskite structure. Given the comparatively complicated diffraction patterns, it was relatively difficult to refine the phase composition using the Rietveld method.

SOFC electrodes should be operated at elevated temperatures and typically under an air atmosphere. The phase structure of perovskite materials at elevated temperatures is then more worthy to be paid attention. The ordering of oxygen vacancies that appear at room temperature may be disturbed at high temperatures, thereby resulting in the transformation of the superlattice structure to an oxygen vacancy-disordered structure, thus introducing oxygen-ion conductivity into the oxides. The phase structure of BF was then investigated in air at elevated temperatures by HT-XRD. As shown in Figure 2, BF had diffraction patterns that were more similar to those of a

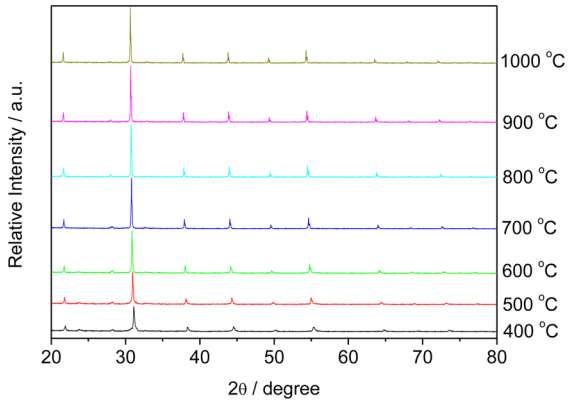

Figure 2. HT-XRD patterns of BF powder between 400 and 1000 °C under an air atmosphere.

cubic perovskite phase at elevated temperatures (within the range from 400 to 1000 °C) than at room temperature. As noted earlier,[18] the as-prepared BF powder at room temperature actually consisted of a mixture of cubic phase $BaFeO_3$, orthorhombic phase $BaFe_2O_4$, and monoclinic phase $Ba_2Fe_2O_5$, in which the percentage of $BaFeO_3$ was just 41.4%. On the basis of the in situ XRD patterns, the relative intensity of the diffraction peaks corresponding to the $BaFe_2O_4$ and $Ba_2Fe_2O_5$ phases decreased with increasing temperature. The characteristic peaks of the $Ba_2Fe_2O_5$ phase almost completely vanished at higher temperatures, whereas the cubic $BaFeO_3$ phase became predominant, and its content increased with increasing temperature, as indicated by the increasing intensity of the related peaks. In actuality, the very small amounts of $BaCO_3$ constituent also existed in the sample so that the orthorhombic phase $BaFe_2O_4$ could be transformed to the cubic phase $BaFeO_3$ at higher temperatures. Although minute amounts of $BaCO_3$ or BaO indeed existed in the sample at more elevated temperatures, the levels of $BaCO_3$ or BaO constituent might be too minute to be detected by the XRD technique. Consequently, the Rietveld refinement of XRD patterns at higher temperatures could not provide relevant information on the $BaCO_3$ or BaO constituent. At 700 °C, for example, the BF powder consisted of a major $BaFeO_3$ cubic phase (91.6(2) wt %), which exhibited a primitive lattice in the $Pm3m$ space group with a lattice parameter of a = 4.122(6) Å (Figure 3a). To obtain further structural information about the high temperature phase, the sample was quenched under the same temperature and atmosphere conditions and was subjected to high-resolution TEM (HR-TEM). HR-TEM in conjunction with selected area electron diffraction (SAED) also revealed that the sample mainly contained an oxygen vacancy-disordered perovskite oxide with cubic lattice symmetry (Figure 3b). The minor phase (8.(3) wt %) was identified as an orthorhombic $BaFe_2O_4$ phase with a $Cmc21$ space group. At higher temperatures, e.g., 900 °C, the content of the overwhelmingly predominant cubic $BaFeO_3$ phase was even higher, reaching 94.4(0) wt %. It suggests that, at more elevated temperatures, BF oxide was almost a pure cubic perovskite phase. The refined phase composition and lattice parameters of BF oxide at higher temperatures, as well as the obtained reliability factors of the refinements, are listed in Table 1.

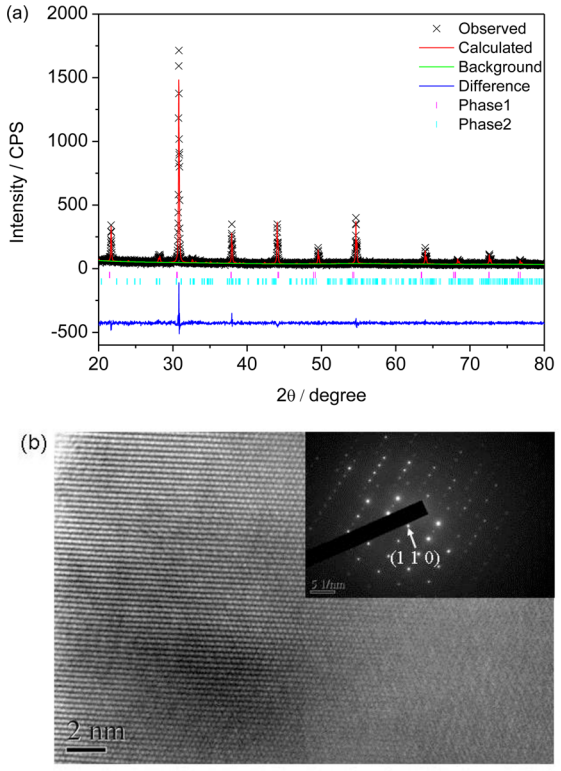

Figure 3. Crystal structure of BF at 700 °C. (a) Rietveld refinement of in situ XRD patterns; (b) HR-TEM image of the major phase shows cubic perovskite structure, and the inset depicts the SAED pattern.

The results above demonstrate that, within the intermediate temperature range and under open circuit or modest polarization (500−750 °C, P_{O_2} = 0.21−10^{-5} atm) conditions, BF did not possess a single oxygen vacancy disordered cubic perovskite phase structure; instead, it was a mixture of an oxygen-ion conducting phase (cubic phase) and a nonconductive phase ($BaFe_2O_4$). The apparent oxygen-ion conductivity for mixed conducting oxides with overwhelming electronic conductivity can be obtained from the oxygen permeation flux of the corresponding membrane. At elevated temperatures, if there is an oxygen potential gradient across a membrane made from such mixed conducting materials, oxygen from the oxygen rich side can permeate in the form of oxygen ions through the membrane bulk to the oxygen lean side to establish a steady oxygen flux. The oxygen permeation flux can be expressed by the following equation:

$$J_{O_2}(\mathrm{mL\cdot cm^{-2}\cdot min^{-1}}, [\mathrm{STP}]) = \left(C_O - \frac{0.21}{0.79}\cdot C_N \cdot \sqrt{\frac{28}{32}}\right)\cdot\frac{Q}{S} \quad (1)$$

where C_O and C_N are the measured gas-phase concentrations of oxygen and nitrogen, respectively, in the sweeping gas; Q is the flow rate (mL min^{-1}) of the permeate stream, and S is the effective surface area (cm^2) exposed to the sweeping gas. Assuming that bulk diffusion controls the oxygen permeation flux, the average oxygen-ion conductivity can be calculated using the Wagner relation, which is shown in eq 2, based on the measured oxygen flux.

$$J_{O_2} = \frac{RT\sigma_i}{16F^2L}\ln\frac{p_h}{p_l} \quad (2)$$

where R is the gas constant, T is the absolute temperature, F is the Faraday constant, L is the thickness of the membrane, and p_h and p_l are the partial oxygen pressures on the feed and permeate sides, respectively.

Shown in Figure 4 is the temperature dependence of the oxygen permeation fluxes for SC, BC, SF, and BF membranes

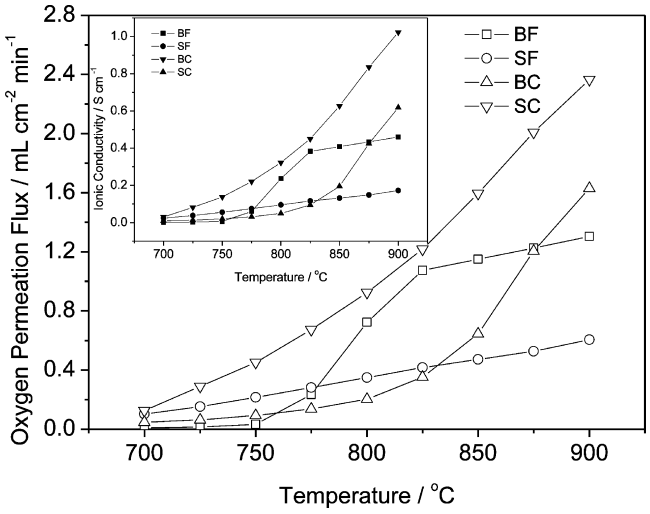

Figure 4. Temperature dependence of oxygen permeation fluxes for BF, SF, BC, and SC membranes. The inset is the temperature dependence of calculated oxygen-ion conductivities for BF, SF, BC, and SC materials based on the measured oxygen permeation fluxes.

and the calculated oxygen-ion conductivities (Figure 4 inset). For all four membranes, a near zero oxygen permeation flux was observed at temperatures below 750 °C, suggesting the lack of long oxygen diffusion paths in these materials at temperatures below 750 °C. It might be explained by the presence of

Table 1. Two-Phase Rietveld Refinement Results for BF: Phases A and B[a]

	700 °C		800 °C		900 °C	
	A	B	A	B	A	B
a (Å)	4.122(6)	8.60(4)	4.131(7)	8.72(0)	4.140(5)	8.72(4)
b (Å)		19.2(9)		18.9(1)		18.9(8)
c (Å)		5.47(1)		5.50(6)		5.45(4)
weight ratio (wt %)	91.6(2)	8.(3)	92.9(7)	7.(0)	94.4(0)	5.6(0)
χ^2	0.9093		0.9450		1.032	
Rp (%)	10.75		10.96		11.52	
Rwp (%)	13.5		13.83		14.46	

[a]Phase A, cubic $BaFeO_3$ in the *Pm*3*m* space group; phase B, orthorhombic $BaFe_2O_4$ in the *Cmc*21 space group.

an oxygen-ion insulating phase (such as $BaFe_2O_4$ in BF sample) that mixed with the oxygen-ion conducting phase (cubic $BaFeO_3$ in BF sample) to block the long-range diffusion of oxygen ions within the oxide bulk. Similar conclusions were also reached for SC, BC, and SF oxides. Only at adequate temperatures could the insulating phase in these undoped parent oxides be transformed by degrees into an oxygen vacancy-disordered cubic phase to then make the oxides conductive for oxygen ions at long range.

The TGA profile (in air) and the corresponding O_2-TPD curve (under flowing helium) of BF are shown in Figure 5a,b,

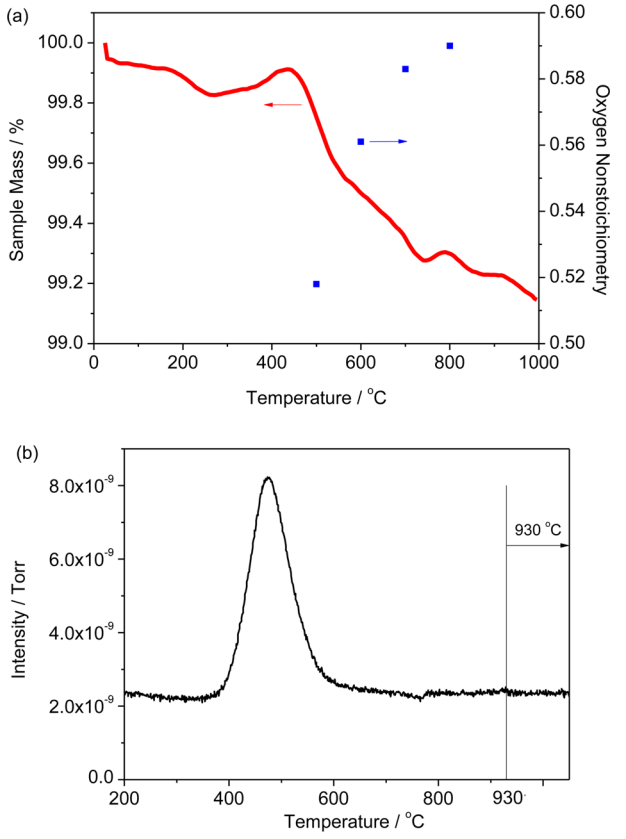

Figure 5. (a) The thermal analysis and oxygen nonstoichiometry (in air) of BF as a function of temperature; (b) the corresponding O_2-TPD curve (under flowing helium) of BF.

respectively. In the TGA profile, an initial weight loss at temperatures below 100 °C (∼−0.07%) and a gradual weight loss starting from 100 °C up to 300 °C (∼−0.10%) with an accelerated weight loss at temperatures above 200 °C were observed. Interestingly, a weight gain was observed from approximately 300 °C until approximately 420 °C (∼+0.08%). From 420 °C on, a steady decrease in weight was observed (∼−0.79%). From the O_2-TPD curve, it can be clearly observed that the loss of lattice oxygen (under helium atmosphere) started at a temperature of approximately 400 °C. It suggests the weight loss in air at temperatures below 300 °C in the TGA profile was due to the release of weakly and strongly surface adsorbed water. The weight gain between 300 and 420 °C suggests that the as-obtained BF was oxidized by air within this temperature range. At temperatures above 420 °C, the BF started to be thermally reduced.

Because the A-site of the perovskite oxides were totally replaced by either Ba^{2+} or Sr^{2+} with a low valence state (2+), such oxides usually possess very high oxygen vacancy concentrations; in actuality, the as-reported oxygen nonstoichiometry (δ) of the above four oxides in the literature has varied from 0.0 to 1.0, depending on the synthetic conditions.[19−22] It is generally believed that a high oxygen vacancy concentration within the temperature range of cell operation is beneficial for oxygen-ion conduction since it is the oxygen-ion charge carrier, thus contributing to the superior electrochemical performance at intermediate temperatures. Thus, the oxygen nonstoichiometry values concentrated over the intermediate-temperature range between 500 and 800 °C need to be specifically investigated since it is the working temperature of the electrode material. Nevertheless, the phase composition in BF sample varies from minute to minute with the increasing temperature and it is hardly refined using the Rietveld method at each elevated temperature point. Therefore, the oxygen nonstoichiometry values can barely be available as a continuous function of temperature during the cell operation. The temperatures within the range of 500−800 °C at intervals of 100 °C are selected as experimental points. After refining the phase compositions of the HT-XRD patterns for BF sample, on the basis of the TGA data and the nonstoichiometry at room temperature, the high-temperature oxygen nonstoichiometry of the sample was obtained by applying the principle of average valence state and unchanged molar weight of iron ions in BF sample with the results also shown in Figure 5a. The oxygen vacancy concentration (δ) became as high as 0.50−0.60 under the fuel cell operating conditions.

3.2. Electrochemical Activity. The electrochemical activity of BF for ORR was first tested by applying symmetric cells with SDC as the electrolyte. Shown in Figure 6a are the typical EIS of the BF in a Nyquist plot. It shows suppressed semi arcs, which can be fitted by an equivalent circuit as shown in the Figure 6a inset. Typically, an arc at high frequency is related to the charge transfer process, an arc at intermediate frequency is associated with the surface diffusion process, and an arc at low frequency is caused by concentration polarization.[23] In this study, such a low frequency arc did not appear, suggesting the absence of gas diffusion polarization. It suggests that the as-fabricated BF electrode possessed sufficient porosity to ensure free gas diffusion. The charge transfer polarization resistance overwhelmed the diffusion polarization resistance, indicating that the charge transfer process was the main rate limiting step for ORR over BF electrode. Anyway, it is very surprising to find that BF electrode possessed a low overall polarization resistance. For example, it was only 0.011 Ω cm^2 at 750 °C and 0.43 Ω cm^2 at 550 °C. Such values were highly encouraging by considering the cobalt-free nature and the poor apparent oxygen-ion conductivity inside the oxide bulk within such a temperature range. The temperature dependences of ASRs over BF, SC, BF, and SF electrodes are shown in Figure 6b; by comparison, the ASRs of the benchmark BSCF electrode with high oxygen-ion conductivity and the conventional LSM and $LaFeO_{3-\delta}$ (LF) electrode were also presented. Even at temperatures as low as 500 °C, an ASR of 1.89 Ω cm^2 was still achieved for the BF electrode. Compared to that of the benchmark BSCF electrode, the ASRs obtained from SC, BC, SF, and BF electrodes were still highly attractive and were only modestly larger at corresponding temperatures. However, for the LSM, which had both negligible oxygen-ion conductivity and zero oxygen vacancy concentration, very large ASRs were observed; for example, a value of ∼76.5 Ω cm^2 was reached even at 700 °C, which was approximately 3000 times that of BF

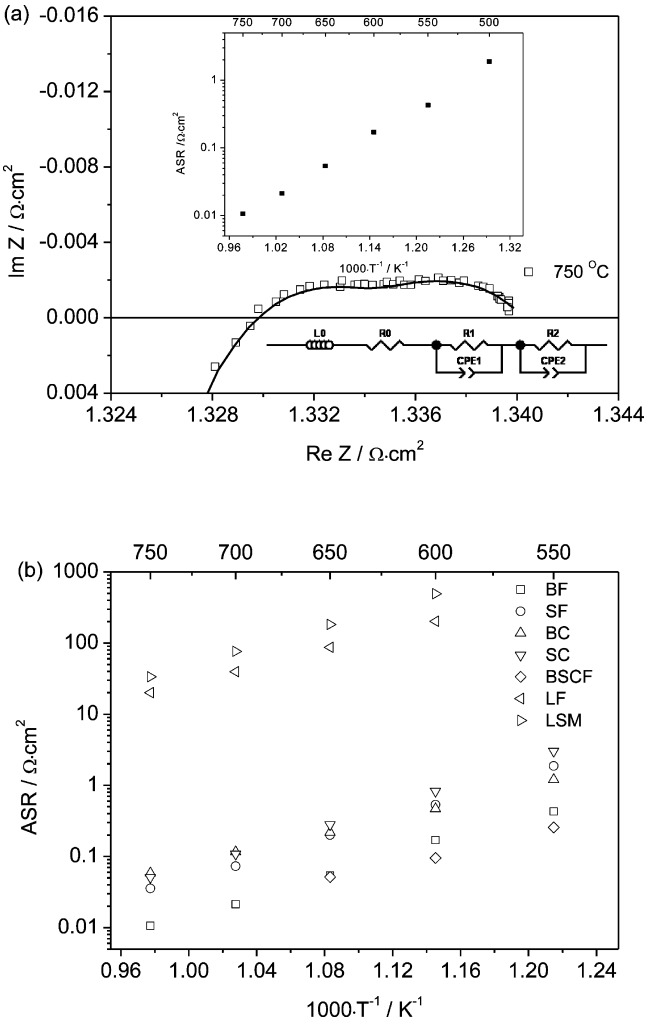

Figure 6. (a) The typical Nyquist impedance plot for the symmetric cell BF|SDC|BF measured at 750 °C. The insets are testing temperature dependence of the ASR for BF between 500 and 750 °C and the equivalent circuit adopted for fitting the EIS data. (b) The temperature dependences of the ASRs over BF, SF, BC, SC, benchmark BSCF, and conventional LSM and LF electrodes.

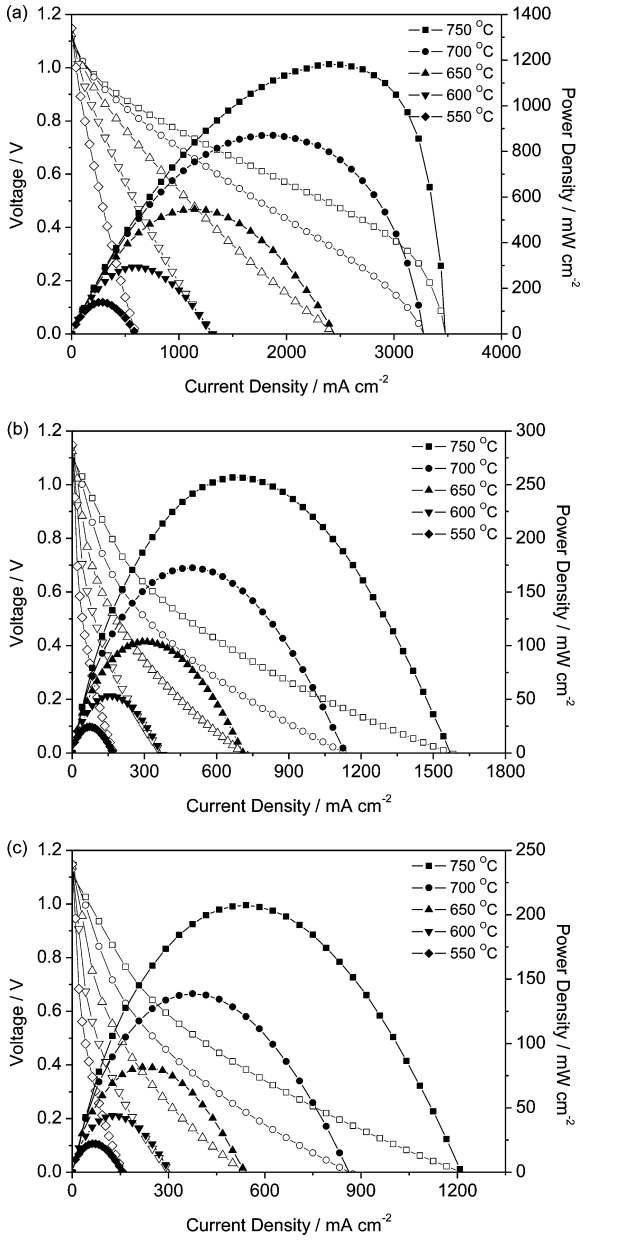

Figure 7. Typical *I*−*V* and *I*−*P* polarization curves of the various cells with different cathodes: (a) BF; (b) LSM; (c) LF.

electrode at the same temperature. The ASRs of LF were also much higher than that of BF but somewhat lower than that of LSM.

The electrode performance of BF was further investigated in complete cells. A single cell was fabricated with NiO+ YSZ anode, thin-film YSZ electrolyte (∼15 μm), SDC buffer layer (∼5 μm), and BF cathode. For performance testing, the anode chamber was fed with hydrogen while the cathode side was exposed to ambient air. To allow for comparison, similar cells with LSM and LF cathodes were also fabricated and tested. Shown in Figure 7 are the typical *I*−*V* and *I*−*P* polarization curves of the various cells with different cathodes. Maximum power densities of 1180, 870, 546, 293, and 139 mW cm^{-2} were achieved at 750, 700, 650, 600, and 550 °C, respectively, for the cell with BF cathode, which are highly attractive and comparable to similar cells with other high-performance cobalt-free cathodes.[24−26] For comparison, a similar cell with LSM electrode exhibited PPDs of 256, 172, 103, 53, and 24 mW cm^{-2} at the same corresponding temperatures above, while the values were 206, 138, 81, 44, and 22 mW cm^{-2} for a similar cell with the LF electrode. These results further demonstrate the high performance of the BF electrode for ORR, even in real fuel cells.

3.3. Origin of High Activity. Oxygen reduction over an electrode involves several substeps, including gas phase diffusion, surface adsorption, oxygen dissociation, charge transfer, surface diffusion of adsorbed molecular oxygen, dissociated atomic oxygen or any charged oxygen species, incorporation of oxygen ions into the electrolyte or electrode, diffusion of oxygen ions within the electrode bulk (assuming that the electrode material has oxygen-ion conductivity), and/or diffusion of oxygen ions through the electrodelelectrolyte interface.[27] Except for gas phase diffusion, all other steps are closely related to the composition of electrode. For simplicity, the ORR can be separated into the surface diffusion process (e.g., surface adsorption, surface dissociation, and surface diffusion) and the charge transfer process. The beneficial effect of introducing oxygen-ion conductivity into the electrode

dx.doi.org/10.1021/am502240m | ACS Appl. Mater. Interfaces 2014, 6, 11180−11189

material is to increase the active reaction sites for charge transfer and to effectively shorten the distance for surface diffusion.

The catalytic activity of perovskite oxides for oxygen activation is usually determined by the B-site cations.[28] On the basis of the investigations above, it is clear that iron and cobalt exhibited better catalytic activity for ORR than did manganese. However, the much better performance of BF than LSM cannot simply be explained by a difference in the B-site cations because both LF and BF contained iron in the B-site of their perovskite lattices, but a much better performance for ORR was observed for BF than for LF. In the past, considerable efforts have been made to stabilize the oxygen vacancy disordered cubic lattice structure by doping the A-site, B-site, or both sites of these parent oxides with the proper cations.[18,29,30] For example, we have recently demonstrated the slight doping of the A-site of BF with La^{3+} to form $Ba_{0.95}La_{0.05}FeO_{3-\delta}$, which can effectively stabilize the cubic structure down to room temperature; the oxide possessed very high oxygen permeation flux to perform as a ceramic membrane and high activity for ORR to act as an electrode.[18] However, because the oxygen ions in BF were immobilized over a long-range at intermediate temperatures due to the presence of a nonconductive phase inside the oxide, the much better activity of BF than LF and LSM could not be explained by the oxygen-ion conductivity. Actually, the high performance of cation-ordered double perovskite oxides with the general formula of $LnBaCo_2O_{5+\delta}$ for ORR strongly suggests that high oxygen-ion conductivity is sometimes not the most critical point for achieving high electrochemical activity for ORR.[31−33] $LnBaCo_2O_{5+\delta}$ oxides are a special type of conducting oxides with two-dimensional oxygen diffusion paths, which exhibited very high oxygen diffusivity at the $a-b$ planes of approximately several orders of magnitude greater than in the direction perpendicular to the $a-b$ planes (c plane) as well as very high oxygen surface exchange kinetics.[34] These materials usually possess a polycrystalline structure, and their actual apparent oxygen-ion conductivities could be much lower than that measured from single crystals. Indeed, under similar conditions (e.g., membrane thickness, oxygen gradient, and oxygen partial pressures at both membrane sizes), by using such polycrystalline oxides as dense oxygen-permeating membranes, the oxygen fluxes were much lower than that through the BSCF membrane, which had a cubic lattice perovskite structure that allowed for free oxygen diffusion in all three dimensions.[31] Interestingly, by using such double perovskite oxides, in particular $PrBaCo_2O_{5+\delta}$, as the electrode, a similar electrode activity for ORR compared to BSCF electrode was achieved at intermediate temperatures.[35] It suggests that, once the surface exchange kinetics is fast enough, the oxygen bulk diffusion could have less effect on the activity of the electrode material for ORR.

To obtain information about the oxygen surface exchange kinetics of BF electrode, we tried to use the ECR technique; LSM and LF samples were also measured for comparison. By suddenly changing the surrounding atmosphere of the sample bar with an oxygen partial pressure of P_{O_2}' to another atmosphere with an oxygen partial pressure of P_{O_2}'', a new equilibrium of the oxygen vacancy concentration inside the oxide lattice is progressively established. A change in the oxygen vacancy concentration inside the oxide lattice will be accompanied by a change in the electrical conductivity of the sample. The information about the surface exchange and bulk diffusion could then be determined from the ECR data. Shown in Figure 8 are the ECR curves of BF at various temperatures.

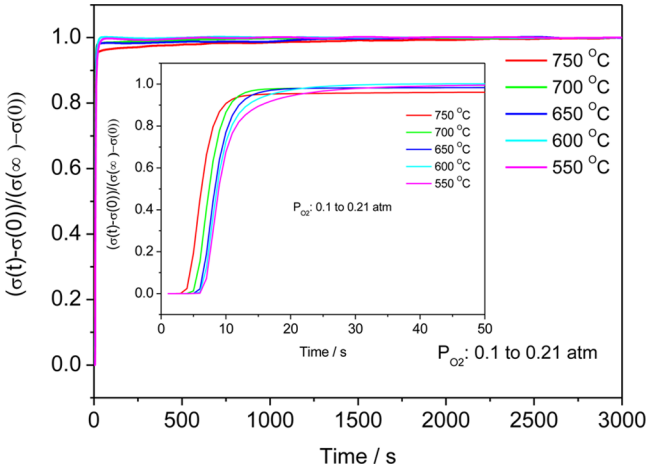

Figure 8. ECR response curves of BF at various temperatures after a sudden change in the oxygen partial pressure from 0.1 to 0.21 atm.

The D_{chem} and K_{chem} of LF and LSM at 750 °C were measured and are listed in Table 2; the results from the literature for

Table 2. Oxygen Bulk Diffusion Coefficient D_{chem} and Surface Exchange Coefficient K_{chem} of LF, LSM, and BSCF at 750 °C Measured by the ECR Technique

	LF	LSM	BSCF
D_{chem} ($cm^2\ s^{-1}$)	6.8×10^{-6}		2.3×10^{-4} [36]
K_{chem} ($cm\ s^{-1}$)	5.6×10^{-5}		2.4×10^{-3} [36]

BSCF are also presented for comparison.[36] The insensitivity of the conductivity of LSM with respect to an abrupt change in the oxygen partial pressure of the surrounding atmosphere resulted in failure in obtaining D_{chem} and K_{chem} values via the ECR measurements. Anyway, it is predictable that LSM exhibited both very slow oxygen bulk diffusion rate and very sluggish oxygen surface exchange kinetics. The electrical conductivity of LF exhibited greater sensitivity toward the change in the oxygen partial pressure of the surrounding atmosphere than that of LSM. The derived D_{chem} and K_{chem} values of LF from the ECR curve reached 6.8×10^{-6} $cm^2\ s^{-1}$ and 5.6×10^{-5} $cm\ s^{-1}$, respectively, at 750 °C. Compared to the values of BSCF, the corresponding values of LF are approximately 2 orders of magnitude lower. Surprisingly, it only took approximately 50 s for the electrical conductivity of BF to reach a new equilibrium after a sudden change in the oxygen partial pressure of the surrounding atmosphere from 0.1 to 0.21 atm. It indicates that BF had very fast surface exchange kinetics to allow for quick buildup of a new equilibrium in the new environment. However, it is difficult to obtain D_{chem} and K_{chem} values accurately derived from the ECR curves due to their large difference. It has been suggested that a large error could be obtained under the condition of the ratio of D_{chem} to K_{chem} being markedly different from the smallest dimension of the bar-shaped sample.[37]

To obtain more information about the surface exchange kinetics of BF electrode, TG analysis was also performed by suddenly changing the oxygen partial pressure of the surrounding atmosphere at a fixed temperature. The TGA

profile of BF, which is shown in Figure 9, was first heated up to 700 °C at a rate of 10 °C min^{-1} and maintained at this

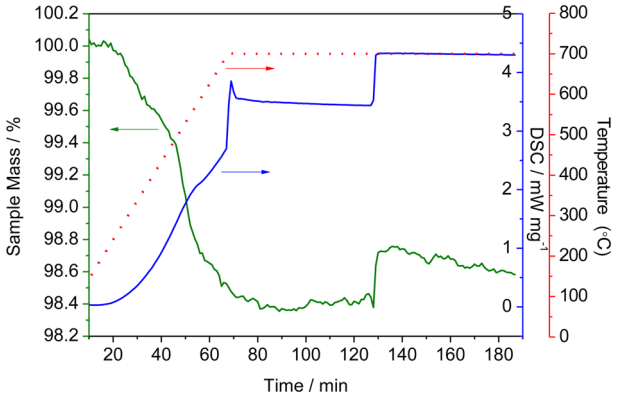

Figure 9. Thermal analysis of BF as a function of temperature and time after a sudden change in the oxygen partial pressure from 10^{-5} to 0.21 atm.

temperature for 1 h under a nitrogen atmosphere (P_{O_2} = 10^{-5} atm) to balance the weight, and then, the atmosphere was suddenly changed to a nitrogen−oxygen gas mixture with an oxygen partial pressure of 0.21 atm. After the sudden change in atmosphere, a quick weight gain was observed in the TG profile, suggesting the fast oxidation of BF by the surrounding atmosphere had occurred. Actually, it only took approximately 3 min for the weight to reach a new balance, which is much shorter than the time required for many other perovskite materials, as reported in the literature.[38,39] Similar to ORR over an electrode, the oxidation of BF involves surface adsorption of molecular oxygen, dissociation, charge transfer, diffusion of oxygen into the oxide bulk, and simultaneous oxidation of iron in the oxide lattice to a higher oxidation state. The fast establishment of a new equilibrium weight after the sudden change in the surrounding atmosphere suggests that BF had very fast oxygen surface exchange kinetics and that the oxidation state of iron is very easily changed.

The reaction for the reduction of oxygen to oxygen ions over an iron-containing electrode can be written as $(1/2)O_2 + V_O^{\bullet\bullet} + 2Fe^{x+} \rightarrow O^{2-} + 2Fe^{(x+1)+}$, which indicates that the ORR requires both oxygen vacancies and redox capability of iron. The main difference between BF and LF is their oxygen vacancy concentrations. Although both LF and BF had a similar oxidation state of ∼3.0 for iron, LF had almost no oxygen vacancies in the bulk at both room and elevated temperatures, whereas the oxygen vacancy concentration (δ) in BF became as high as 0.58 at 700 °C. The low oxygen vacancy concentration thus significantly limited the ORR over the LF electrode. As for LSM, it has been reported that the oxygen nonstoichiometry was still near zero for oxygen partial pressures ranging from 0.21 to 10^{-5} atm,[40] indicating that it is difficult to change the oxidation state of manganese in LSM. The lack of oxygen vacancies and the poor redox of manganese in LSM resulted in poor activity of LSM for ORR. Regarding BF, although there was also a lack of long oxygen diffusion paths inside the oxide bulk, the high oxygen vacancy concentration as demonstrated by iodometric titration and TGA, as well as the easy redox of iron cations as supported by TGA and O_2-TPD, facilitated the reduction of oxygen to oxygen ions. As a result, the charge transfer polarization resistance over BF electrode was relatively low, as demonstrated by EIS. The high oxygen vacancy concentration may also favor oxygen surface adsorption and dissociation because oxygen vacancies can provide active sites, while the interaction between oxygen and oxygen vacancies can weaken the O−O bond and thus promote breakage of the O−O bond. Consequently, a relatively low surface diffusion polarization resistance was also observed. The combination of high charge transfer and oxygen surface diffusion then led to favorable activity of BF for ORR, although there were few long-range bulk diffusion paths for oxygen.

On the basis of the analysis above, a probable mechanism for the high activity of BF for ORR was proposed and is schematically shown in Figure 10. Additionally, the presence

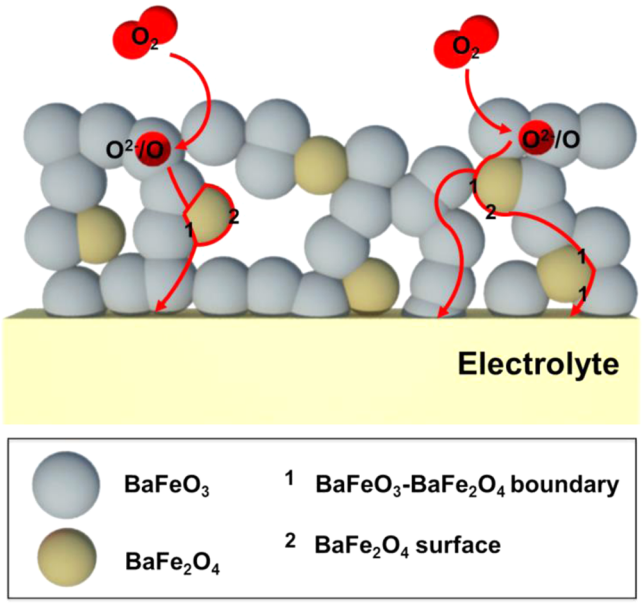

Figure 10. Schematic diagram of the oxygen surface diffusion and charge transfer processes for BF electrode.

of the two phase $BaFeO_3/BaFe_2O_4$ domains in the BF sample was revealed through the HR-TEM analysis (Figure S1, Supporting Information). At intermediate operating temperatures, BF was actually composed of a highly conducting oxygen-ion $BaFeO_3$ phase and a nonionic conductive $BaFe_2O_4$ phase. Although the amount of $BaFe_2O_4$ in the sample was relatively small, it significantly blocked oxygen ions transport from one $BaFeO_3$ grain to another; as a result, the material exhibited poor apparent oxygen-ion conductivity at intermediate temperatures. However, the high oxygen vacancy concentration and fast surface exchange kinetics of the cubic $BaFeO_3$ phase resulted in very high activity for oxygen activation. The $BaFeO_3$ phase in BF electrode thus provided the main active sites for the activation of oxygen with the formation of charged or noncharged oxygen species, which then might diffuse through the $BaFeO_3$−$BaFe_2O_4$ grain boundary or the $BaFe_2O_4$ surface to an adjacent $BaFeO_3$ grain and finally to the electrolyte surface. Charge transfer over the cubic $BaFeO_3$ phase was relatively easy because of its high oxygen vacancy concentration and the ease with which the iron ions changed oxidation states, whereas the nonconductive $BaFe_2O_4$ phase might perform for surface oxygen diffusion; as a result, the electrode exhibited favorably low polarization resistance for both charge transfer and surface diffusion processes.

4. CONCLUSIONS

In summary, we have presented the surprisingly high performance for ORR of a parent oxide BF that lacks long-range oxygen-ion diffusion paths. The results presented herein show that superior electrocatalytic activity can be achieved in BF-derived SOFCs due to the easy redox of iron cations and the very fast oxygen surface exchange kinetics (strongly correlated with the surface oxygen vacancy concentration) of the BF oxide, although it had no long-range bulk oxygen diffusion paths. A probable mechanism was proposed and was used to illustrate the high electrocatalytic activity of BF for ORR. The novel characteristics of the oxide catalyst provide a new promising strategy for the development of high-performance oxygen reduction electrodes for SOFCs.

■ ASSOCIATED CONTENT

Ⓢ Supporting Information

HR-TEM characterization for revealing the presence of the two phase $BaFeO_3/BaFe_2O_4$ domains. This material is available free of charge via the Internet at http://pubs.acs.org.

■ AUTHOR INFORMATION

Corresponding Author

*E-mail: shaozp@njtech.edu.cn. Tel.: +86 25 83172256. Fax: +86 25 83172242.

Notes

The authors declare no competing financial interest.

■ ACKNOWLEDGMENTS

This work was supported by the "National Science Foundation for Distinguished Young Scholars of China" under contract No. 51025209.

■ REFERENCES

(1) Shao, Z. P.; Haile, S. M.; Ahn, J.; Ronney, P. D.; Zhan, Z. L.; Barnett, S. A. A Thermally Self-Sustained Micro Solid-Oxide Fuel-Cell Stack with High Power Density. *Nature* **2005**, *435*, 795−798.

(2) McIntosh, S.; Gorte, R. J. Direct Hydrocarbon Solid Oxide Fuel Cells. *Chem. Rev.* **2004**, *104*, 4845−4866.

(3) McPhee, W. A. G.; Boucher, M.; Stuart, J.; Parnas, R. S.; Koslowske, M.; Tao, T.; Wilhite, B. A. Demonstration of a Liquid-Tin Anode Solid-Oxide Fuel Cell (LTA-SOFC) Operating from Biodiesel Fuel. *Energy Fuels* **2009**, *23*, 5036−5041.

(4) Zhou, W.; Sunarso, J.; Zhao, M. W.; Liang, F. L.; Klande, T.; Feldhoff, A. A Highly Active Perovskite Electrode for the Oxygen Reduction Reaction Below 600 °C. *Angew. Chem., Int. Ed.* **2013**, *52*, 14036−14040.

(5) Yang, W.; Hong, T.; Li, S.; Ma, Z. H.; Sun, C. W.; Xia, C. R.; Chen, L. Q. Perovskite $Sr_{1-x}Ce_xCoO_{3-\delta}$ ($0.05 \leq x \leq 0.15$) as Superior Cathodes for Intermediate Temperature Solid Oxide Fuel Cells. *ACS Appl. Mater. Interfaces* **2013**, *5*, 1143−1148.

(6) Murray, E. P.; Barnett, S. A. (La, Sr)MnO_3-(Ce, Gd)O_{2-x} Composite Cathodes for Solid Oxide Fuel Cells. *Solid State Ionics* **2001**, *143*, 265−273.

(7) Liang, F. L.; Chen, J.; Jiang, S. P.; Chi, B.; Pu, J.; Li, J. High Performance Solid Oxide Fuel Cells with Electrocatalytically Enhanced (La, Sr)MnO_3 Cathodes. *Electrochem. Commun.* **2009**, *11*, 1048−1051.

(8) Wang, W.; Jiang, S. P. Effect of Polarization on the Electrode Behavior and Microstructure of (La, Sr)MnO_3 Electrodes of Solid Oxide Fuel Cells. *J. Solid State Electrochem.* **2004**, *8*, 914−922.

(9) Haanappel, V. A. C.; Mertens, J.; Rutenbeck, D.; Tropartz, C.; Herzhof, W.; Sebold, D.; Tietz, F. Optimisation of Processing and Microstructural Parameters of LSM Cathodes to Improve the Electrochemical Performance of Anode-Supported SOFCs. *J. Power Sources* **2005**, *141*, 216−226.

(10) Shao, Z. P.; Haile, S. M. A High-Performance Cathode for the Next Generation of Solid-Oxide Fuel Cells. *Nature* **2004**, *431*, 170−173.

(11) Gangopadhayay, S.; Inerbaev, T.; Masunov, A. E.; Altilio, D.; Orlovskaya, N. Structural Characterization Combined with the First Principles Simulations of Barium/Strontium Cobaltite/Ferrite as Promising Material for Solid Oxide Fuel Cells Cathodes and High-Temperature Oxygen Permeation Membranes. *ACS Appl. Mater. Interfaces* **2009**, *1*, 1512−1519.

(12) Lynch, M. E.; Yang, L.; Qin, W. T.; Choi, J. J.; Liu, M. F.; Blinn, K.; Liu, M. L. Enhancement of $La_{0.6}Sr_{0.4}Co_{0.2}Fe_{0.8}O_{3-\delta}$ Durability and Surface Electrocatalytic Activity by $La_{0.85}Sr_{0.15}MnO_{3\pm\delta}$ Investigated Using a New Test Electrode Platform. *Energy Environ. Sci.* **2011**, *4*, 2249−2258.

(13) Yang, Y.; Jiang, Y. S.; Wang, Y. W.; Sun, Y. B. Photoinduced Decomposition of $BaFeO_3$ During Photodegradation of Methyl Orange. *J. Mol. Catal. A: Chem.* **2007**, *270*, 56−60.

(14) Xian, H.; Zhang, X. W.; Li, X. G.; Li, L. Y.; Zou, H. H.; Meng, M.; Li, Q.; Tan, Y. S.; Tsubaki, N. $BaFeO_{3-x}$ Perovskite: An Efficient NO_x Absorber with a High Sulfur Tolerance. *J. Phys. Chem. C* **2010**, *114*, 11844−11852.

(15) Hayashi, N.; Yamamoto, T.; Kageyama, H.; Nishi, M.; Watanabe, Y.; Kawakami, T.; Matsushita, Y.; Fujimori, A.; Takano, M. $BaFeO_3$: A Ferromagnetic Iron Oxide. *Angew. Chem., Int. Ed.* **2011**, *50*, 12547−12550.

(16) Zhang, K.; Ran, R.; Ge, L.; Shao, Z. P.; Jin, W. Q.; Xu, N. P. Systematic Investigation on New $SrCo_{1-y}Nb_yO_{3-\delta}$ Ceramic Membranes with High Oxygen Semi-Permeability. *J. Membr. Sci.* **2008**, *323*, 436−443.

(17) Zhou, W.; Ge, L.; Chen, Z. G.; Liang, F. L.; Xu, H. Y.; Motuzas, J.; Julbe, A.; Zhu, Z. H. Amorphous Iron Oxide Decorated 3D Heterostructured Electrode for Highly Efficient Oxygen Reduction. *Chem. Mater.* **2011**, *23*, 4193−4198.

(18) Dong, F. F.; Chen, D. J.; Chen, Y. B.; Zhao, Q.; Shao, Z. P. La-doped $BaFeO_{3-\delta}$ Perovskite as a Cobalt-Free Oxygen Reduction Electrode for Solid Oxide Fuel Cells with Oxygen-Ion Conducting Electrolyte. *J. Mater. Chem.* **2012**, *22*, 15071−15079.

(19) Mori, S. Phase Transformation in Barium Orthoferrate, $BaFeO_{3-x}$. *J. Am. Ceram. Soc.* **1966**, *49*, 600−605.

(20) Takeda, Y.; Kanno, K.; Takada, T.; Yamamoto, O.; Takano, M.; Nakayama, N.; Bando, Y. Phase Relation in the Oxygen Non-stoichiometric System, $SrFeO_x$ ($2.5 \leq x \leq 3.0$). *J. Solid State Chem.* **1986**, *63*, 237−249.

(21) Strauss, S. W.; Fankuchen, I.; Ward, R. Barium Cobalt Oxide of the Perowskite Type. *J. Am. Chem. Soc.* **1951**, *73*, 5084−5086.

(22) Vashook, V. V.; Zinkevich, M. V.; Zonov, Y. G. Phase Relations in Oxygen-Deficient $SrCoO_{2.5-\delta}$. *Solid State Ionics* **1999**, *116*, 129−138.

(23) Adler, S. B.; Lane, J. A.; Steele, B. C. H. Electrode Kinetics of Porous Mixed-Conducting Oxygen Electrodes. *J. Electrochem. Soc.* **1996**, *143*, 3554−3564.

(24) Niu, Y. J.; Zhou, W.; Sunarso, J.; Ge, L.; Zhu, Z. H.; Shao, Z. P. High Performance Cobalt-Free Perovskite Cathode for Intermediate Temperature Solid Oxide Fuel Cells. *J. Mater. Chem.* **2010**, *20*, 9619−9622.

(25) Jiang, S. S.; Zhou, W.; Niu, Y. J.; Zhu, Z. H.; Shao, Z. P. Phase Transition of a Cobalt-Free Perovskite as a High-Performance Cathode for Intermediate-Temperature Solid Oxide Fuel Cells. *ChemSusChem* **2012**, *5*, 2023−2031.

(26) Dong, F. F.; Chen, Y. B.; Ran, R.; Chen, D. J.; Tadé, M. O.; Liu, S. M.; Shao, Z. P. $BaNb_{0.05}Fe_{0.95}O_{3-\delta}$ as a New Oxygen Reduction Electrocatalyst for Intermediate Temperature Solid Oxide Fuel Cells. *J. Mater. Chem. A* **2013**, *1*, 9781−9791.

(27) Zhou, W.; Ran, R.; Shao, Z. P. Progress in Understanding and Development of $Ba_{0.5}Sr_{0.5}Co_{0.8}Fe_{0.2}O_{3-\delta}$-Based Cathodes for Intermediate-Temperature Solid-Oxide Fuel Cells: A Review. *J. Power Sources* **2009**, *192*, 231−246.

(28) Nitadori, T.; Ichiki, T.; Misono, M. Catalytic Properties of Perovskite-Type Mixed Oxides (ABO_3) Consisting of Rare Earth and

3d Transition Metals. The Roles of the A- and B-site Ions. *Bull. Chem. Soc. Jpn.* **1988**, *61*, 621−626.
(29) Wang, F. C.; Chen, D. J.; Shao, Z. P. Composition and Microstructure Optimization and Operation Stability of Barium Deficient $Ba_{1-x}Co_{0.7}Fe_{0.2}Nb_{0.1}O_{3-\delta}$ Perovskite Oxide Electrodes. *Electrochim. Acta* **2013**, *103*, 23−31.
(30) Efimov, K.; Halfer, T.; Kuhn, A.; Heitjans, P.; Caro, J.; Feldhoff, A. Novel Cobalt-Free Oxygen-Permeable Perovskite-Type Membrane. *Chem. Mater.* **2010**, *22*, 1540−1544.
(31) Zhang, K.; Ge, L.; Ran, R.; Shao, Z. P.; Liu, S. M. Synthesis, Characterization and Evaluation of Cation-Ordered $LnBaCo_2O_{5+\delta}$ as Materials of Oxygen Permeation Membranes and Cathodes of SOFCs. *Acta Mater.* **2008**, *56*, 4876−4889.
(32) Kim, J. H.; Mogni, L.; Prado, F.; Caneiro, A.; Alonso, J. A.; Manthiram, A. High Temperature Crystal Chemistry and Oxygen Permeation Properties of the Mixed Ionic-Electronic Conductors $LnBaCo_2O_{5+\delta}$ (Ln= Lanthanide). *J. Electrochem. Soc.* **2009**, *156*, B1376−B1382.
(33) Chen, D. J.; Ran, R.; Shao, Z. P. Assessment of $PrBaCo_2O_{5+\delta}$ + $Sm_{0.2}Ce_{0.8}O_{1.9}$ Composites Prepared by Physical Mixing as Electrodes of Solid Oxide Fuel Cells. *J. Power Sources* **2010**, *195*, 7187−7195.
(34) Kim, G.; Wang, S.; Jacobson, A. J.; Reimus, L.; Brodersen, P.; Mims, C. A. Rapid Oxygen Ion Diffusion and Surface Exchange Kinetics in $PrBaCo_2O_{5+x}$ with a Perovskite Related Structure and Ordered A Cations. *J. Mater. Chem.* **2007**, *17*, 2500−2505.
(35) Chen, D. J.; Ran, R.; Zhang, K.; Wang, J.; Shao, Z. P. Intermediate-Temperature Electrochemical Performance of a Polycrystalline $PrBaCo_2O_{5+\delta}$ Cathode on Samarium-Doped Ceria Electrolyte. *J. Power Sources* **2009**, *188*, 96−105.
(36) Chen, D. J.; Shao, Z. P. Surface Exchange and Bulk Diffusion Properties of $Ba_{0.5}Sr_{0.5}Co_{0.8}Fe_{0.2}O_{3-\delta}$ Mixed Conductor. *Int. J. Hydrogen Energy* **2011**, *36*, 6948−6956.
(37) Lane, J. A.; Kilner, J. A. Measuring Oxygen Diffusion and Oxygen Surface Exchange by Conductivity Relaxation. *Solid State Ionics* **2000**, *136*, 997−1001.
(38) Zeng, Y.; Lin, Y. S. A Transient TGA Study on Oxygen Permeation Properties of Perovskite-Type Ceramic Membrane. *Solid State Ionics* **1998**, *110*, 209−221.
(39) Remsen, S.; Dabrowski, B. Synthesis and Oxygen Storage Capacities of Hexagonal $Dy_{1-x}Y_xMnO_{3+\delta}$. *Chem. Mater.* **2011**, *23*, 3818−3827.
(40) Jiang, S. P. Development of Lanthanum Strontium Manganite Perovskite Cathode Materials of Solid Oxide Fuel Cells: A Review. *J. Mater. Sci.* **2008**, *43*, 6799−6833.